NASA/TM-2000-210328

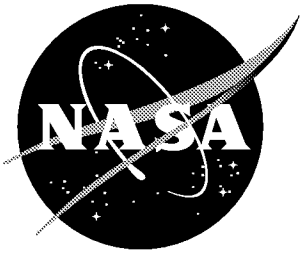

A Comparison of Analytical and Experimental Data for a Magnetic Actuator

Nelson J. Groom
Langley Research Center, Hampton, Virginia

V. Dale Bloodgood, Jr.
Old Dominion University, Norfolk, Virginia

September 2000

The NASA STI Program Office ... in Profile

Since its founding, NASA has been dedicated to the advancement of aeronautics and space science. The NASA Scientific and Technical Information (STI) Program Office plays a key part in helping NASA maintain this important role.

The NASA STI Program Office is operated by Langley Research Center, the lead center for NASA's scientific and technical information. The NASA STI Program Office provides access to the NASA STI Database, the largest collection of aeronautical and space science STI in the world. The Program Office is also NASA's institutional mechanism for disseminating the results of its research and development activities. These results are published by NASA in the NASA STI Report Series, which includes the following report types:

- TECHNICAL PUBLICATION. Reports of completed research or a major significant phase of research that present the results of NASA programs and include extensive data or theoretical analysis. Includes compilations of significant scientific and technical data and information deemed to be of continuing reference value. NASA counterpart of peer-reviewed formal professional papers, but having less stringent limitations on manuscript length and extent of graphic presentations.

- TECHNICAL MEMORANDUM. Scientific and technical findings that are preliminary or of specialized interest, e.g., quick release reports, working papers, and bibliographies that contain minimal annotation. Does not contain extensive analysis.

- CONTRACTOR REPORT. Scientific and technical findings by NASA-sponsored contractors and grantees.

- CONFERENCE PUBLICATION. Collected papers from scientific and technical conferences, symposia, seminars, or other meetings sponsored or co-sponsored by NASA.

- SPECIAL PUBLICATION. Scientific, technical, or historical information from NASA programs, projects, and missions, often concerned with subjects having substantial public interest.

- TECHNICAL TRANSLATION. English-language translations of foreign scientific and technical material pertinent to NASA's mission.

Specialized services that complement the STI Program Office's diverse offerings include creating custom thesauri, building customized databases, organizing and publishing research results ... even providing videos.

For more information about the NASA STI Program Office, see the following:

- Access the NASA STI Program Home Page at ***http://www.sti.nasa.gov***

- E-mail your question via the Internet to help@sti.nasa.gov

- Fax your question to the NASA STI Help Desk at (301) 621-0134

- Phone the NASA STI Help Desk at (301) 621-0390

- Write to:
  NASA STI Help Desk
  NASA Center for AeroSpace Information
  7121 Standard Drive
  Hanover, MD 21076-1320

NASA/TM-2000-210328

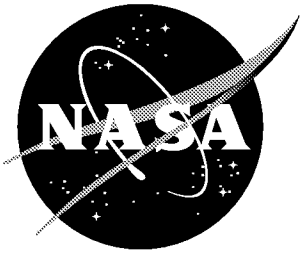

A Comparison of Analytical and Experimental Data for a Magnetic Actuator

Nelson J. Groom
Langley Research Center, Hampton, Virginia

V. Dale Bloodgood, Jr.
Old Dominion University, Norfolk, Virginia

National Aeronautics and
Space Administration

Langley Research Center
Hampton, Virginia 23681-2199

September 2000

Available from:

NASA Center for AeroSpace Information (CASI)
7121 Standard Drive
Hanover, MD 21076-1320
(301) 621-0390

National Technical Information Service (NTIS)
5285 Port Royal Road
Springfield, VA 22161-2171
(703) 605-6000

SUMMARY

Theoretical and experimental force-displacement and force-current data are compared for two configurations of a simple horseshoe, or bipolar, magnetic actuator. One configuration utilizes permanent magnet wafers to provide a bias flux and the other configuration has no source of bias flux. The theoretical data are obtained from two analytical models of each configuration. One is an ideal analytical model which is developed under the following assumptions: (1) zero fringing and leakage flux, (2) zero actuator coil mmf loss, and (3) infinite permeability of the actuator core and suspended element flux return path. The other analytical model, called the extended model, is developed by adding loss and leakage factors to the ideal model. The values of the loss and leakage factors are calculated from experimental data. The experimental data are obtained from a magnetic actuator test fixture, which is described in detail. Results indicate that the ideal models for both configurations do not match the experimental data very well. However, except for the range around zero force, the extended models produce a good match. The best match is produced by the extended model of the configuration with permanent magnet flux bias.

INTRODUCTION

This paper presents theoretical and experimental force-displacement and force-current data for two configurations of a simple horseshoe, or bipolar, magnetic actuator. One configuration utilizes permanent magnet wafers to provide a bias flux and the other configuration has no source of bias flux. The theoretical data are obtained from two analytical models of each configuration. One is an ideal analytical model which is developed under the following assumptions: (1) zero fringing and leakage flux, (2) zero actuator coil mmf loss, and (3) infinite permeability of the actuator core and suspended element flux return path. The ideal models for each configuration are developed using the approach detailed in reference 1. The other analytical model, called the extended model, is developed by adding loss and leakage factors to the ideal model. The values of the loss and leakage factors are calculated from experimental data. The experimental data are obtained from a magnetic actuator test fixture, which is described in detail.

ANALYTICAL MODELS

In this section analytical models of two configurations of a simple horseshoe, or bipolar, magnetic actuator are developed. One configuration, shown schematically in figure 1, has no source of bias flux. The other configuration, shown schematically in figure 2, utilizes permanent magnet wafers mounted on the pole faces to provide a bias flux. The analytical models consist of an ideal model and an extended model. The ideal model is developed using the approach detailed in reference 1 under the following assumptions: (1) zero fringing and leakage flux, (2) zero actuator coil mmf loss, and (3) infinite actuator core and suspended element flux return path permeability. The extended model is developed by adding loss and leakage factors to the ideal model.

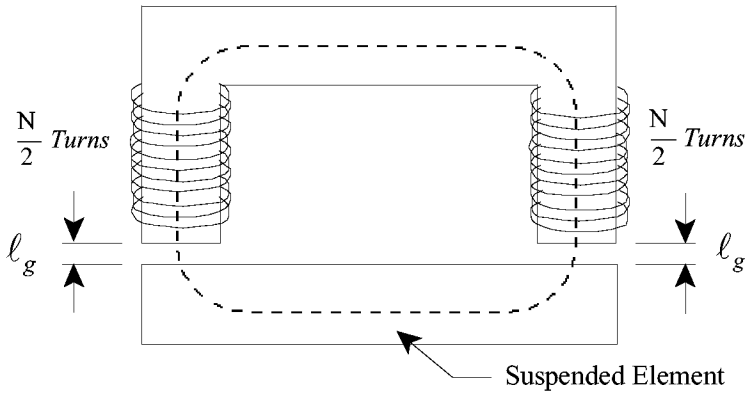

Figure 1.- Magnetic Actuator with No Flux Bias

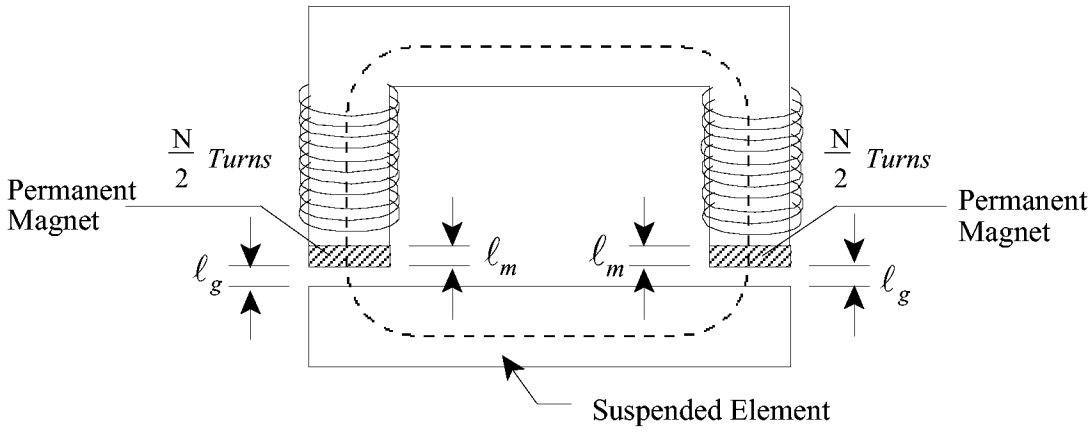

Figure 2.- Magnetic Actuator with Permanent Magnet Flux Bias

Magnetic Actuator With No Flux Bias

Ideal Model.- Taking the line integral around the contour shown in figure 1 results in

$$\oint_C H \bullet d\ell = 2H_g\ell_g + H_a\ell_a + H_s\ell_s \tag{1}$$

where H_g is the magnetic field intensity in the air gap, ℓ_g is the length of one air gap, H_a is the magnetic field intensity in the actuator core, ℓ_a is the length of the contour in the actuator core, H_s is the magnetic field intensity in the suspended element, and ℓ_s is the length of the contour in the suspended element. Magnetic actuators are designed to operate about a nominal specified gap, which will be defined as g_0. If up is defined as positive in figure 1, the air gap length, ℓ_g, can be written in terms of g_0 as

$$\ell_g = g_0 - x \tag{2}$$

where x is the displacement of the suspended element with respect to g_0. Using the relationship

$$\oint_C H \bullet d\ell = \int_S J \bullet n da \tag{3}$$

results in

$$2H_g\ell_g + H_a\ell_a + H_s\ell_s = Ni \tag{4}$$

Using the constitutive relationship

$$B = \mu H \tag{5}$$

where μ is the permeability of the media being considered, equation (4) can be written as

$$2B_g\ell_g + \mu_0\left(\left(\frac{B_a}{\mu_a}\right)\ell_a + \left(\frac{B_s}{\mu_s}\right)\ell_s\right) = \mu_0 Ni \tag{6}$$

Since μ_a and μ_s are assumed to be infinite and B_a and B_s are finite inside the actuator core and suspended element flux return path, the term $\mu_0\left(\left(\frac{B_a}{\mu_a}\right)\ell_a + \left(\frac{B_s}{\mu_s}\right)\ell_s\right)$ becomes zero. Solving for the magnetic flux density in the actuator gaps results in

$$B_g = \frac{\mu_0 Ni}{2\ell_g} \tag{7}$$

From reference 1 the force produced by the magnetic actuator can be written as

$$F_m = \frac{\mu_0 A_g (Ni)^2}{4\ell_g^2} \tag{8}$$

Using equation (7), the force as a function of flux density becomes

$$F_m = \frac{B_g^2 A_g}{\mu_0} \tag{9}$$

Extended Model.- In a typical magnetic actuator with a ferromagnetic core and suspended element flux return path, the permeability is relatively large but finite. Also, there are actuator coil mmf losses. In order to account for these effects, loss factors can be added to the ideal model. Since the permeability of the core and suspended element flux return path is large, the term $\mu_0\left(\left(\frac{B_a}{\mu_a}\right)\ell_a + \left(\frac{B_s}{\mu_s}\right)\ell_s\right)$ is relatively small and can be combined with the term $2B_g\ell_g$ and accounted for by the introduction of the loss factor K_a. To account for actuator coil mmf losses, the loss factor K_i is introduced. Adding K_a and K_i into equation (6) results in

$$2K_a B_g \ell_g = \mu_0 K_i Ni \tag{10}$$

The flux in the gaps becomes

$$B_g = \frac{\mu_0 K_i Ni}{2K_a \ell_g} \tag{11}$$

Equation (11) can be further simplified by defining the combined loss factor, K_L, as

$$K_L = \frac{K_i}{K_a} \tag{12}$$

Equation (11) then becomes

$$B_g = \frac{\mu_0 K_L Ni}{2\ell_g} \tag{13}$$

and the actuator force, from equation (9), becomes

$$F_m = \frac{\mu_0 A_g (K_L Ni)^2}{4\ell_g^2} \tag{14}$$

Magnetic Actuator With Permanent Magnet Flux Bias

Ideal Model.- Using equation (3) and taking the line integral around the contour shown in figure 2 results in

$$2H_g\ell_g + 2H_m\ell_m = Ni \tag{15}$$

In order to determine the permanent magnet operating point, i is set to zero and equation (15) becomes

$$\frac{H_g}{H_m} = -\frac{\ell_m}{\ell_g} \tag{16}$$

Also, the flux in the air gaps is equal to the flux through the permanent magnet wafers

$$B_g A_g = B_m A_m \tag{17}$$

which can be written as

$$\frac{B_g}{B_m} = \frac{A_m}{A_g} \tag{18}$$

Combining (16) and (18) results in

$$\frac{\ell_m}{\ell_g}\left(\frac{A_m}{A_g}\right) = \frac{V_m}{V_g} = -\frac{B_g H_g}{B_m H_m} \tag{19}$$

where V_m and V_g is the volume of the permanent magnet and air gap respectively. A good approximate model for a permanent magnet made of hard magnetic material, such as Samarium Cobalt or Neodymium Iron Boron, is shown in figure (3).

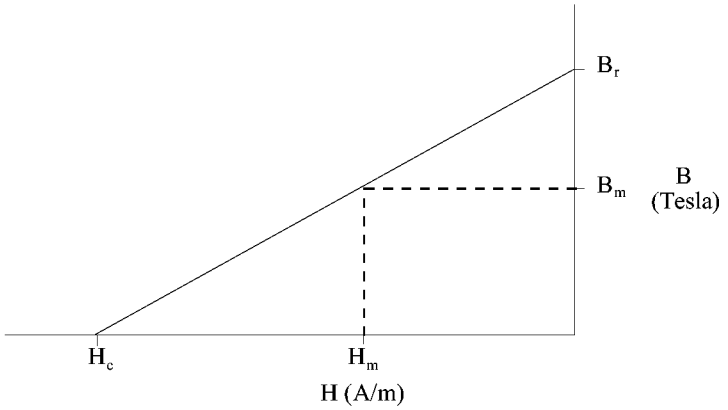

Figure 3.- Ideal B-H Curve For Neodymium Iron Boron

The flux in the magnet can be written as

$$B_m = \mu_m H_m + B_r \tag{20}$$

where $\mu_m = \frac{B_r}{H_c}$, B_r is the residual induction, and H_c is the coercive force. The normal approach in a permanent magnet flux bias design is to minimize the volume of permanent magnet material. From equation (19) it can be seen that in order to minimize V_m, the energy product, $B_m H_m$, must be maximized. Substituting from equation (20), the energy product, $B_m H_m$, becomes

$$B_m H_m = \frac{B_r H_m^2}{H_c} + B_r H_m \tag{21}$$

The energy product is max when $\frac{d(B_m H_m)}{dH_m} = 0$

$$\frac{d(B_m H_m)}{dH_m} = 2\left(\frac{B_r}{H_c}\right) H_m + B_r = 0 \tag{22}$$

From equation (22)

$$H_m = -\frac{H_c}{2} \tag{23}$$

and B_m becomes (from eq. (20))

$$B_m = \frac{B_r}{2} \tag{24}$$

From equations (5) and (16)

$$B_g = -\mu_0 H_m \frac{\ell_m}{\ell_g} \tag{25}$$

Substituting from equation (20) and rearranging terms results in

$$B_g = \frac{\mu_0}{\mu_m}\left(B_r - B_m\right)\frac{\ell_m}{\ell_g} \tag{26}$$

From equation (17)

$$B_g = B_m \frac{A_m}{A_g} \tag{27}$$

In most permanent magnet flux bias actuator designs (including the actuator used in the test fixture described in this paper)

$$A_m = A_g = A_a \tag{28}$$

Also, for permanent magnet material

$$\frac{\mu_0}{\mu_m} \approx 1 \tag{29}$$

Substituting equations (27), (28), and (29) into equation (26) results in

$$B_m = \left(B_r - B_m\right)\frac{\ell_m}{\ell_g} \tag{30}$$

Substituting equation (24) into equation (30) results in

$$\ell_m = \ell_g \tag{31}$$

At the specified operating point, from equation (2), ℓ_m becomes

$$\ell_m = g_0 \tag{32}$$

From equations (5) and (20), equation (15) can be written as

$$2B_g + 2\left(\frac{\mu_0}{\mu_m}\right)(B_m - B_r)\ell_m = \mu_0 Ni \tag{33}$$

Rearranging terms and substituting from equation (17) results in

$$B_g = \frac{\mu_0\left(Ni + 2\left(\frac{\mu_0}{\mu_m}\right)\frac{B_r\ell_m}{\mu_0}\right)}{2\left(\ell_g + \left(\frac{\mu_0}{\mu_m}\right)\left(\frac{A_g}{A_m}\right)\ell_m\right)} \tag{34}$$

Equation (34) can be further simplified by substituting equations (28) and (29)

$$B_g = \frac{\mu_0\left(Ni + \frac{2B_r\ell_m}{\mu_0}\right)}{2\left(\ell_g + \ell_m\right)} \tag{35}$$

The actuator force, from equation (9), becomes

$$F_m = \frac{\mu_o A_g\left(Ni + \frac{2B_r\ell_m}{\mu_0}\right)^2}{4\left(\ell_g + \ell_m\right)^2} \tag{36}$$

Extended Model.- Adding the loss factors K_a and K_i into equation (15) results in

$$2K_a H_g \ell_g + 2H_m\ell_m = K_i Ni \tag{37}$$

In addition to mmf losses, there is also flux leakage. To account for flux leakage, the leakage factor, K_F, is added to equation (17) which results in

$$K_F B_g A_g = B_m A_m \tag{38}$$

Following through the previous development, equation (33) becomes

$$2K_a B_g \ell_g + 2\left(\frac{\mu_0}{\mu_m}\right)(B_m - B_r)\ell_m = \mu_0 K_i Ni \tag{39}$$

and from equation (38), equation (35) becomes

$$B_g = \frac{\mu_0\left(K_i N i + \dfrac{2B_r \ell_m}{\mu_0}\right)}{2\left(K_a \ell_g + K_F \ell_m\right)} \tag{40}$$

From equation (9) the actuator force becomes

$$F_m = \mu_0 A_g \frac{\left(K_i N i + \dfrac{2B_r \ell_m}{\mu_0}\right)^2}{4\left(K_a \ell_g + K_F \ell_m\right)^2} \tag{41}$$

DESCRIPTION OF TEST FIXTURE

A simplified schematic of the magnetic actuator test fixture is shown in Fig. 4.

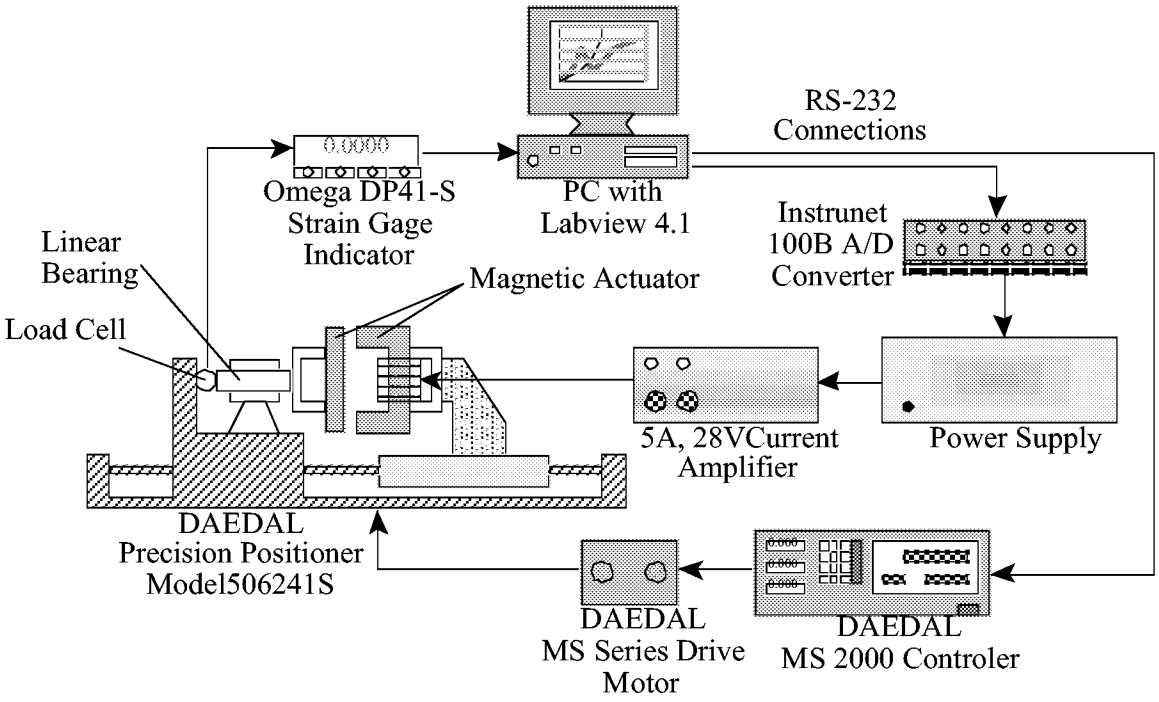

Figure 4.- Schematic Of Magnetic Actuator Test Fixture

The stator was mounted to a precision positioner by an aluminum mounting bracket. The armature was connected to a load cell through an aluminum mounting bracket and aluminum shaft. The shaft was supported by a linear bearing, which restrained the

movement of the armature to 2 degrees-of-freedom, roll about the axial axis of the shaft and lateral movement in the direction of the stator. The shaft was allowed to rotate slightly so that torques would not be transmitted to the load cell, resulting in only the lateral force being measured. The load cell had a maximum range of 50 lb. The positioner was controlled by a PC using Labview 4.1. The signal from the load cell was conditioned by a digital strain gauge indicator and then recorded by Labview. The actual test fixture is shown in Figs. 5 and 6.

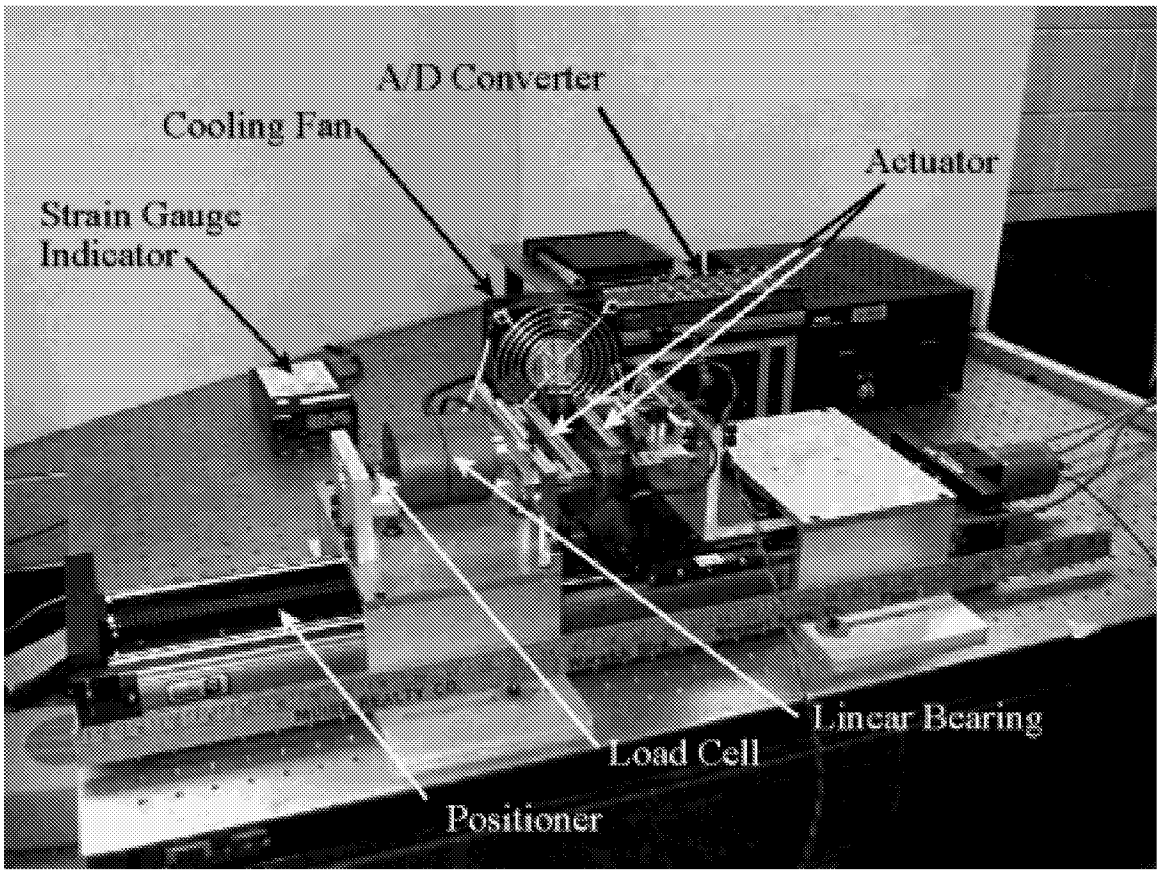

Figure 5.- Magnetic Actuator Test Fixture

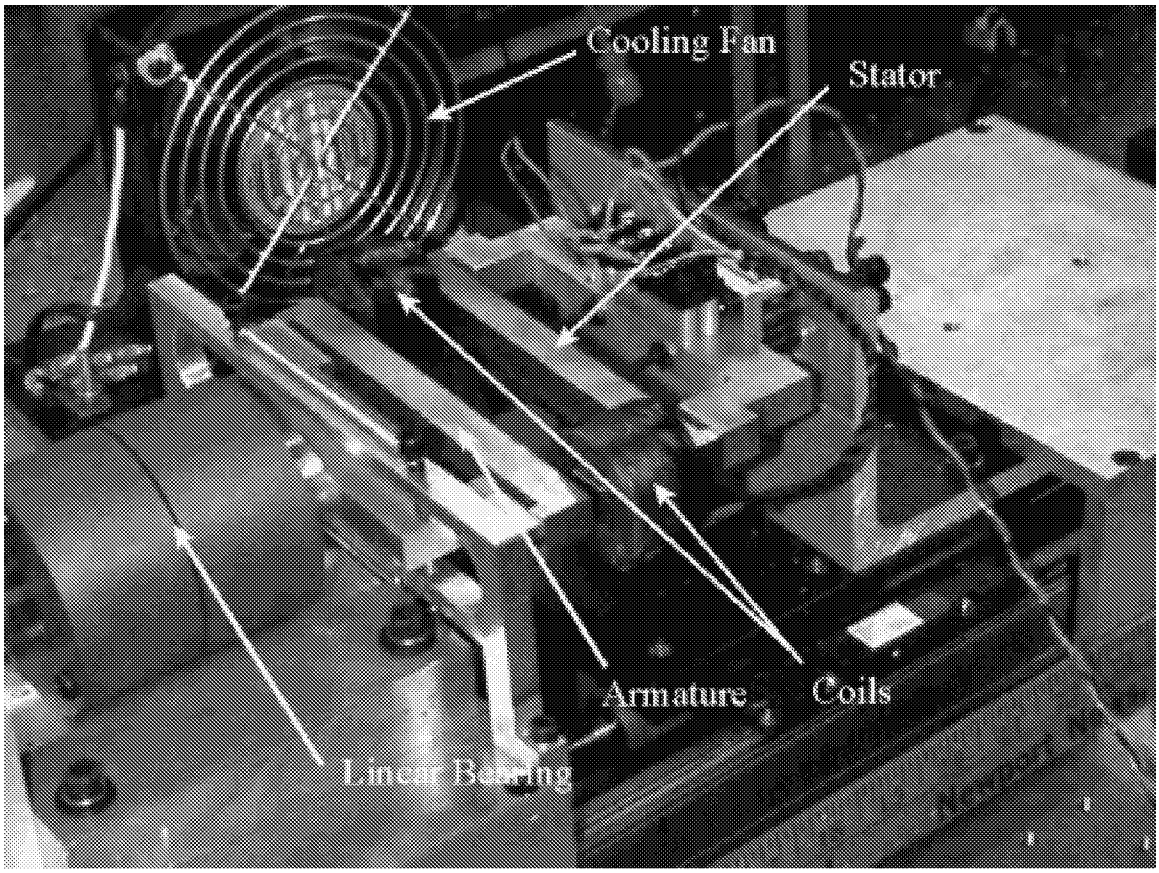

Figure 6.- Magnetic Actuator

The actuator components were constructed from a Connecticut Metal CMI-C cold drawn iron rod. This material is manufactured for use in electromagnetic applications and has a very low carbon content. The B-H curve for the material is shown in Fig. 7. The permanent magnets for the permanent magnet flux bias configuration were constructed of Neodymium-Iron-Boron (Nd-Fe-B) with a residual induction of 1.35 Tesla and a coercivity of -9.7×10^5 A/m. The nominal operating gap for the magnetic actuator was set at 0.05 in. which set the permanent magnet thickness at 0.05 in. also (see eq. 32). The B-H curve for the Nd-Fe-B is shown in Fig. 8.

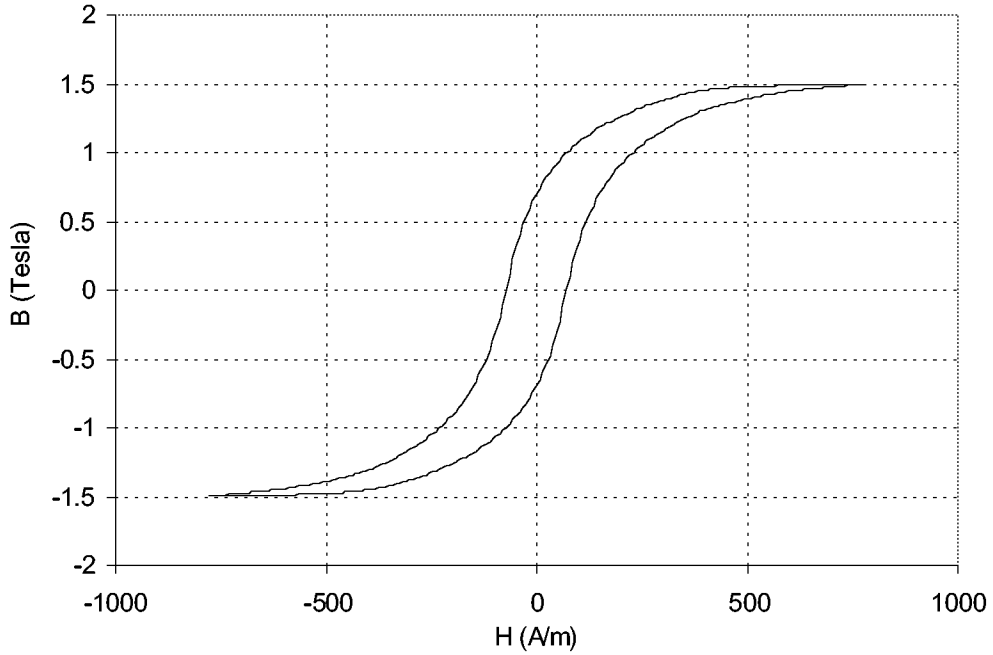

Figure 7.- B-H Curve for Connecticut Steel CMI-C Cold Drawn Steel

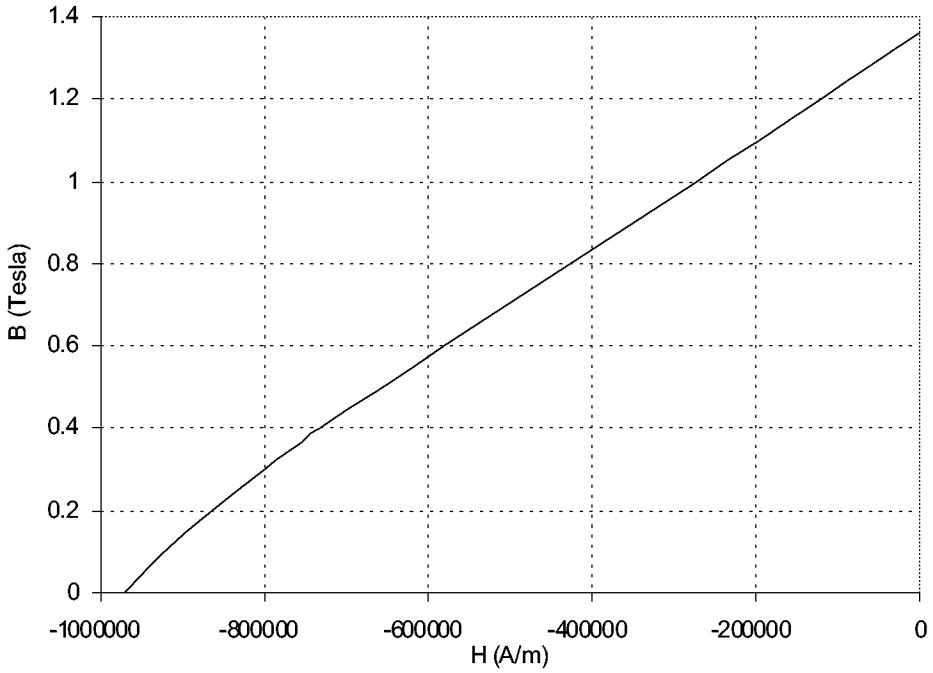

Figure 8.- B-H Curve for Neodymium-Iron-Boron Permanent Magnet

The magnetic actuator design consisted of a simple horseshoe shaped stator and a rectangular armature as shown in Fig. 9.

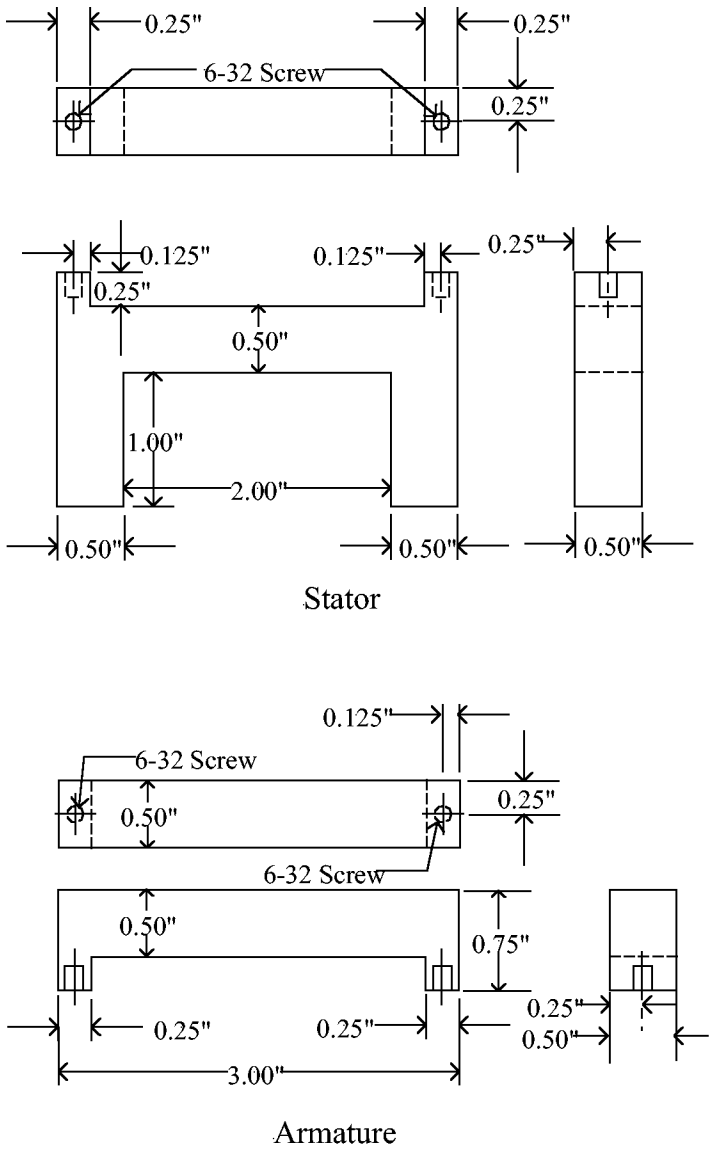

Figure 9.- Design Of Magnetic Actuator Stator and Armature

The stator and the armature had constant cross sectional areas of 0.25 in^2. The stator had a pole separation of 2 inches and a pole length of 1 inch. Both the stator and the armature had extensions located on the back side corners to connect with the aluminum support brackets. These were used to insure that the connection bolts did not reduce the cross sectional area of the magnetic circuit and induce saturation. The connection extensions were located at the edge of the stator and armature to minimize the effect on the magnetic circuit, as is illustrated in Fig. 10.

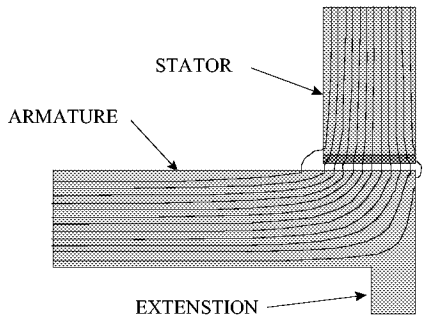

Figure 10.- Magnetic Potential Lines Near Connection Extensions

The magnetic actuator had two coils, one per pole. The coils were connected in series and each coil had 1000 turns. The two coils had resistances of 9.32 Ω and 9.35 Ω.

Each set of measurements was performed five times. The final data presented in Appendix A is the average of the five data sets. The system was calibrated before and after each experiment. The calibration procedure is described in detail in Appendix A. To minimize hysterisis effects, the measurements were recorded in an increasing manner, i.e. the force increment between data points was always positive, except when the force was driven past the zero point of the actuator. The first measurement was taken at the negative limit of the ampere-turns (minimum force) then proceeded to the positive limit (maximum force). For each data point, the system was allowed to settle for 8 seconds to allow the strain gauge signal to settle before the force was recorded.

The zero gap distance was set using the positioner and controller. The two poles of the stator were lined up parallel with the armature. Once the two poles were parallel with the armature, the positioner was advanced in 0.0001 increments toward the armature. For the actuator with no flux bias, the positioner was moved until the armature and stator came in contact and the load cell registered a reading. The positioner was then initialized to zero displacement. For the actuator with flux bias, as the positioner moved the stator toward the armature, the attractive force from the permanent magnet increased. At the point of contact between the stator and the armature the force began to decrease. That point was determined within 0.0001 and the positioner was initialized to zero displacement.

COMPARISON OF IDEAL MODEL AND TEST FIXTURE RESULTS

As mentioned earlier, the nominal operating gap for the magnetic actuator was set at 0.05 in. Therefore, the results presented in the following sections are for this gap length.

Magnetic Actuator With No Flux Bias

A plot of the ideal model and test fixture results for the magnetic actuator with no flux bias is presented in figure 11. A second order trendline is drawn through the test fixture data points.

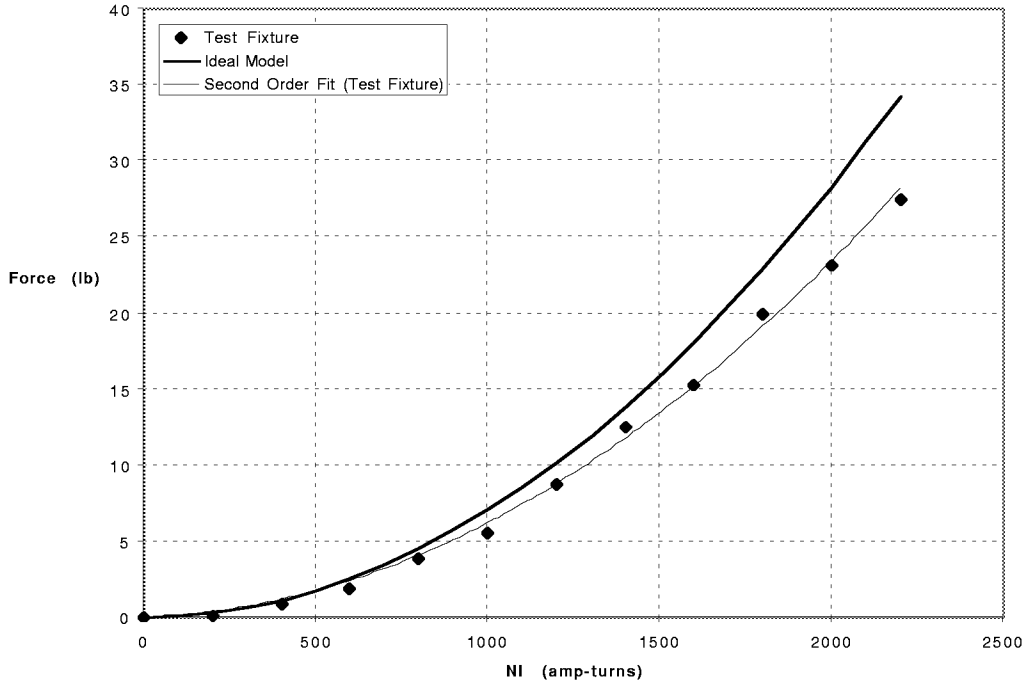

Figure 11.- Ideal Model And Test Fixture Results For Magnetic Actuator with No Flux Bias (ℓ_g = 0.05 in.)

A plot of the percent (%) difference between data points obtained from the test fixture (from the second order trendline) and ideal model is presented in figure 12. The percent difference is defined as

$$\%\ Difference = \left(\frac{F_{fixture} - F_{ideal}}{F_{fixture}} \right) 100 \qquad (42)$$

As can be seen from figure 11, the ideal model results differ significantly from the test fixture results. From figure 12 the percent difference between the test fixture results and the ideal model approaches —22% at Ni = 2200 amp-turns. Since the ideal model predicts a force of 34.2 lb. at Ni = 2200 amp-turns, this translates into a difference of approximately —6.1 lb.

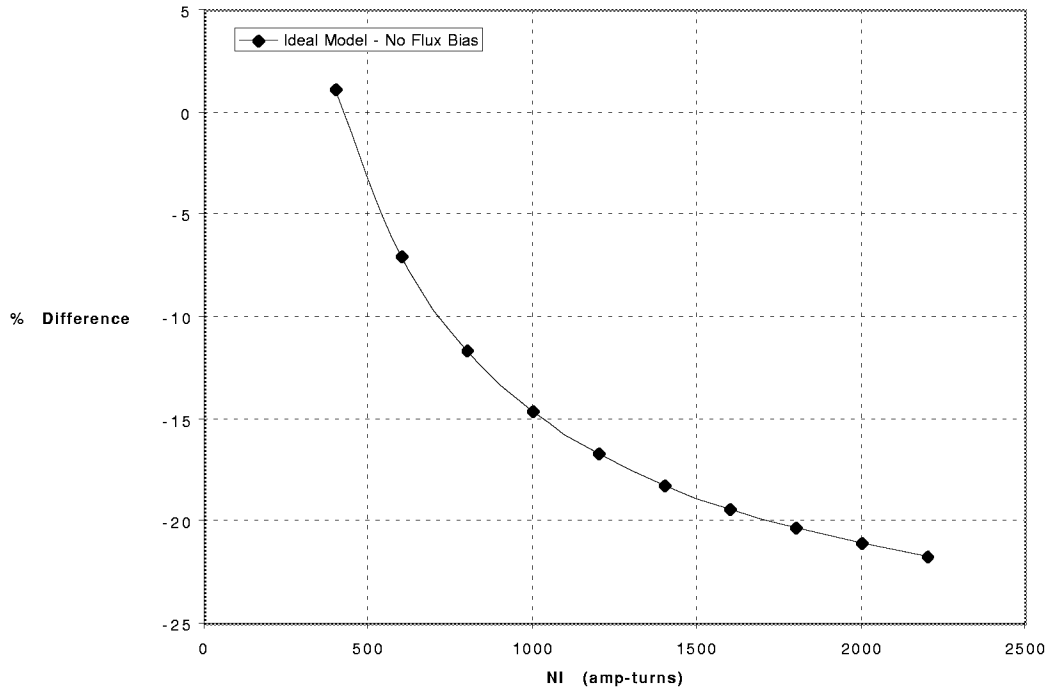

Figure 12.- % Difference Between Test Fixture And Ideal Model Results For Magnetic Actuator With No Flux Bias (ℓ_g = 0.05 in.)

Magnetic Actuator With Permanent Magnet Flux Bias

A plot of the ideal model and test fixture results for the magnetic actuator with permanent magnet flux bias is presented in figure 13. A second order trendline is drawn through the test fixture data points.